ICE, CLOUD, AND LAND ELEVATION SATELLITE-2 (ICESat-2)
ATL12 Ocean Surface Height Release 005/006
Application Notes and Known Issues

Jamie Morison, PSC
Suzanne Dickinson, PSC
David Hancock, GSFC
Leeanne Roberts, GSFC
John Robbins, GSFC

5/5/2023

Release 5.0/6.0

Introduction

This document contains notes for the use of the ICESat-2 ATL12 Ocean Surface Height product. It includes issues that are known to the developers, which may be fixed in future releases of this product. Feedback from the community will be added to future revisions of this document.

Contents

Notes: The ATL12 Ocean Surface Height Product Philosophy and Brief Description

The Ice, Cloud, and Land Elevation Satellite-2 (ICESat-2) provides satellite ocean altimetry unlike any other. ICESat-2 has been developed primarily to measure the height of the Earth's ice and land at high spatial resolution. To achieve this resolution it carries the Advanced Topographic Laser Altimeter System (ATLAS), a photon-counting, multi-beam lidar pulsing at 10 kHz. At the speed of the spacecraft, each beam of ATLAS illuminates 15 m patch of the surface every 0.7 m of along-track distance. Given the low reflectance of the ocean surface, of all the photons detected by ATLAS, on the order of one photon per pulse returns from the ocean surface. ATLAS determines the apparent height of the reflecting surface for each one of these photons along with the apparent height of a lower density of noise photons. Averaged over along-track distance these heights form a histogram of heights reminiscent of the waveforms of other radar (e.g., CryoSat-2) and analog lidar (e.g., ICESat-1) satellite altimeters, and thus we are tempted to think in terms of "retracking" to decide what part of this "waveform" represents the average ocean surface over a "foot print" corresponding to the averaging distance.

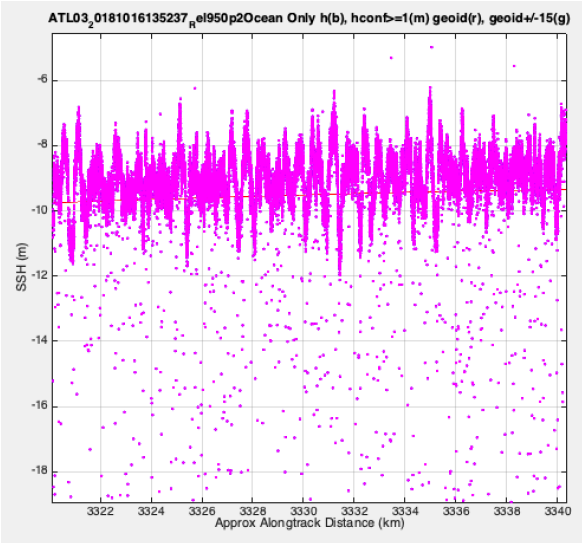

Figure 1. ATL03 photon heights (magenta) from Oct. 16, 2018 over the Pacific Ocean and the EGM2008 geoid (red line). Waves in the dense photon cloud are apparent as well as subsurface and atmospheric noise photons.

We have adopted a different philosophy in processing the ICESat-2. We do not think in terms of "footprint" and "retracking" in the usual way, but treat every photon height documented in the ATL03 data product input to ATL12 as an individual point measurement of surface height averaging less than a meter apart, but with a x-y location uncertainty on the order of 10 m. Figure 1 shows ATL03 photon heights collected over 7-km of ocean surface. The dense cloud of heights representing surface-reflected photons clearly stands out from the lower density of noise photons above and below and reveals surface waves with about 2.5 m significant wave height (SWH) and an apparent 470-m wavelength. In processing, we first distinguish by a histogram trimming method, which of these heights over an adaptively chosen ocean segment length (typically 7-km) are from true surface reflected photons versus noise photons. The resultant "received height histogram" is deconvolved with an instrument impulse response (IIR) histogram representing the height uncertainty associated with the lidar transmit pulse width and other instrumental factors. This produces a surface height histogram that, with its first four moments, is the primary ATL12 products. In addition we analyze the spatial series of surface photons heights to characterize surface waves and calculate the correlation of photon return rate and surface height that constitutes the EM sea state bias (SSB) in the mean sea surface height (SSH).

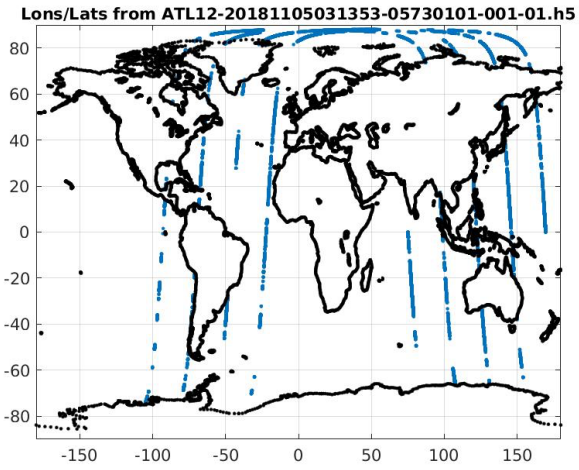

Figure 2. Example of one ATL12 file's worth of ocean segment latitudes and longitudes over four orbits comprising the file.

Thus, the ATL12 Ocean product includes histograms and statistics of sea surface height over variable length along-track ocean segments. The processing has been designed around open ocean conditions and includes a sea state bias calculation. However, the processing is run over the world ocean including ice-covered regions covered by ATL07 and ATL10. In these regions, the statistical products will be valid statistics for the mixed ice-covered and ice-free surface, but mean heights will include the average freeboard of sea ice.

ATL 12 photon heights are derived from the ATL03 ocean photon height data with signal confidence level 1 or higher and within 15 m of the EGM2008 geoid. Signal confidence 2, 3, and 4 correspond to low, medium, and high confidence the photon is surface reflected and confidence level 1 fills a ±15-m buffer about the high confidence level photon heights. This constraint, along with the geoid band criteria, have been found to edit out heights in erroneous downlink bands associated with high background noise rates.

From this population, we first accumulate photon heights likely to fall within the distribution of ocean surface heights until 8,000 candidate photons or 7 km of along-track distance is traversed. All the photons over the resulting ocean segment are then subjected to two iterations selecting photon heights in the histogram at levels above the background rate. After the first iteration, a linear trend and average height is removed from the heights prior to the second iteration. The trend and average height are retained for output as part of the ocean segment statistics. From there the height data follows two paths

The histogram path considers the histogram of the received ocean segment heights and deconvolves the histogram of the instrument impulse response to produce the surface height distribution. This is then fit with a 2 Gaussian mixture to produce the first four moments of the surface height distribution. The derived height surface histogram and the four moments comprise the main the ATL12 data products

The space series track maintains the surface heights as an along-track series and by correlating the photon return rate with surface height at 10-m along-track scale, estimates significant wave height and the EM sea state bias (SSB) ATL12 data products. In future releases, analyses on this track will include more wave properties and estimates of statistical degrees of freedom for the accumulation gridded statistics in the ATL17 gridded data product.

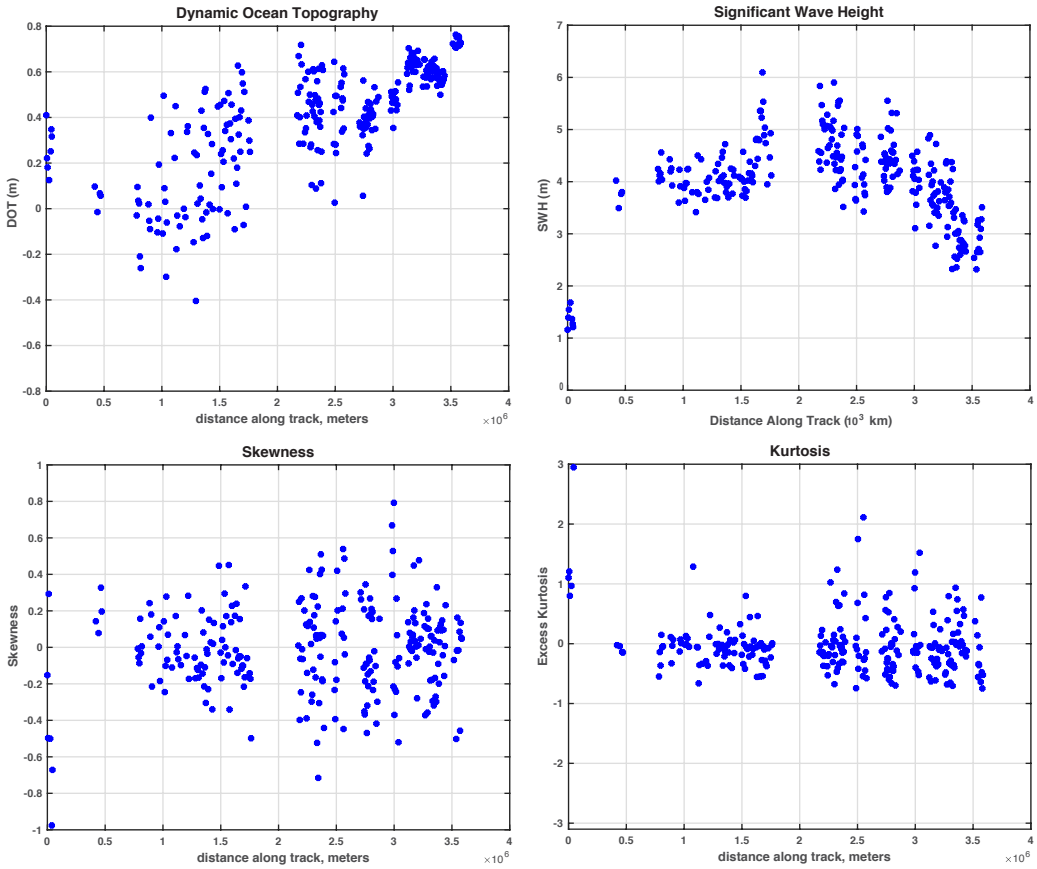

Figure 3. ATL12 ocean segment statistics. Upper left: mean SSH, upper right: significant wave height = 4 x standard deviation, lower left: skewness of sea surface height, lower right: kurtosis of sea surface height. Yellow DOTS are ATL12 ASAS 5.1 and blue dots are from our developmental Matlab code applied to ATL03, which generally does not segment the data exactly the same as ATL12. ASAS 5.1 and Matlab agreement is better where segments are more closely matched.

Each ATL12 data file covers the world ocean over four consecutive ICESat-2 orbits (Fig. 2). ATL12 file names such as ATL12_20181105031353_05730101_001_01.h5 include the date/time sequence (yyyymmddhhmmss=20181105031353) of the start of the first orbit, the reference ground track (_####=_0573), the cycle (##=01), the region (##=01), and the release (###=001).

The processed data are for areas designated as ocean according to the ICESat-2 ocean surface mask. The ocean mask overlaps with the other surface types in buffer zones up to 20-km wide. Consequently, early releases of ATL12 data included bands that were in fact not open ocean but which were close enough to sea level to fall within ±15 m of the geoid, close enough to be accepted by ATL12's processing. Examples were the marginal sea ice zones under the sea ice surface type and low-lying islands under the land surface type. Release 3 processing includes a bathymetry test to ensure the ATL12 processing covers only ocean waters. For each 20-m geo-segment, the corresponding depth from the General Bathymetric Chart of the Oceans (GEBCO, https://www.gebco.net) database is used to determine water depth, and ATL12 processing is done for depths greater than 10-m. As an added benefit, the average GEBCO depth over each ocean segment is output as another Release 3ATL12 data product.

Except in special cases or when overlapping one of the other surface types, over the ocean only the three strong beams with ground tracks separated by 3 km are downlinked by ATLAS. The ATL12 software processes each strong beam independently. An example of ocean statistics measure by the middle strong beam over one ATL03 granule in the North Pacific is shown in Figure 3 for all ocean segments in the granule.

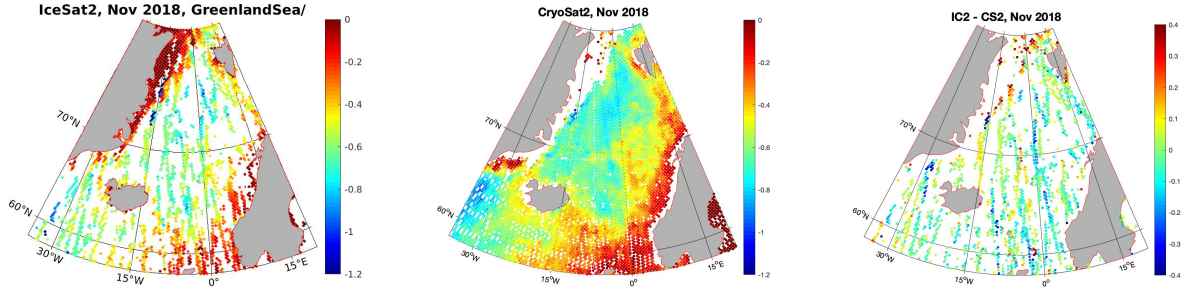

Figure 4. ICESat-2, CryoSat-2 dynamic ocean topography (DOT in meters) comparison for the Greenland Sea in November 2018. Left: ICESat-2 from ATL12 Rel001, bin-averaged in a 25-km grid. In this case ocean and sea ice mask data are included. Center: CryoSat-2 LRM and pLRM from RADS bin-averaged in a 25-km grid. These are open water products. Right: ICESat-2 DOT minus CryoSat-2 DOT bin-averaged in a 25-km grid. Differences are taken only for grid cells with both ICESat-2 and CryoSat-2 data.

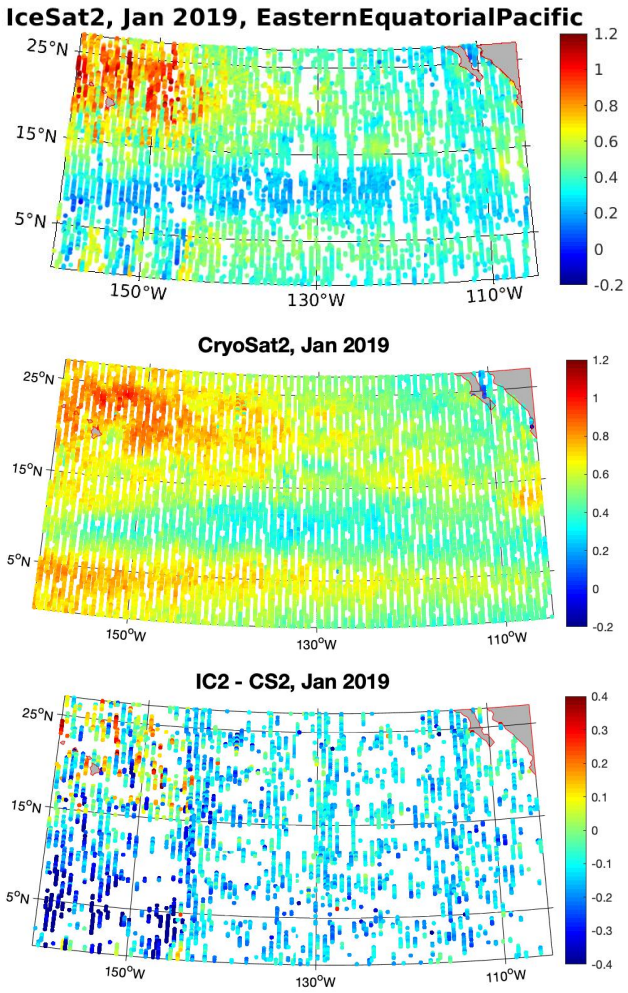

Figure 5. ICESat-2, CryoSat-2 dynamic ocean topography (DOT) comparison for the Eastern Equatorial Pacific in January 2019. Top: ICESat-2 DOT (m) from ATL12 Rel001, bin-averaged in a 25-km grid, Center: CryoSat-2 DOT (m) LRM and pLRM from RADS bin-averaged in a 25-km grid, Bottom: ICESat-2 DOT minus CryoSat-2 DOT (m) bin-averaged in a 25-km grid. Differences are taken only for grid cells with both ICESat-2 and CryoSat-2 data.

Our first efforts at calibration and validation of ICESat-2 SSH show good agreement with CryoSat-2, especially in the Sub-Arctic Seas. Figure 4 shows comparison of ICESat-2 and CryoSat-2 dynamic ocean topography, DOT=SSH-Geoid (EGM08) for the month of November 2018 bin-averaged in a 25-km grid. ICESat-2 did not get as many surface measurements as CryoSat-2, almost surely due cloud cover over the November Greenland Sea. However, the same DOT patterns such as DOT set up towards the coasts associated with the East Greenland, Norwegian, and West Spitzbergen currents are almost identically shown in both data sets. The difference between gridded ICESat-2 and CryoSat-2 DOT is on the right of Figure 4. Over all the grid cells with ICESat-2 and CryoSat-2, ICESat-2 DOT is 0.64 cm higher than CryoSat-2 DOT ± 16.6 cm standard deviation. This comparison is remarkable given the early release of ICESat-2.

Figure 5 is similar to Figure 4 except the comparison is done for the Eastern Equatorial Pacific (EEP) for January 2019. In spite of a lower density of ground tracks at low latitude, ICESAt-2 data coverage in the EEP is arguably better than in the Greenland Sea, likely because of clearer sky conditions. The ICESat-2 and CryoSat-2 DOT patterns in the EEP are very similar, showing among other things the trough along 5°N likely associated with North Equatorial Current and North Equatorial Counter Current. The similarity breaks down a little in the western part of the area with ICESat-2 DOT being a little higher than CryoSat-2 DOT in the northwest and lower than CryoSat-2 DOT in the southwest. On average ICESat-2 DOT is 13.1 cm lower than CryoSat-2 DOT ±12.2 cm standard deviation. This is not as good as the Greenland Sea comparison but comparable in magnitude to other ICESat-2 ground truth comparisons for this release.

Issues

The issues below are those that could affect use of ATL12 Rel. 003 presently or could affect changes in the way ATL12 data are used in the future.

Issue 1. Surface Finding, Subsurface Returns, and Histogram Trimming

Distinguishing surface reflected photon heights involves establishing a histogram of all heights in an ocean segment and then searching outward from the center of the histogram to find high and low limits where the histogram level falls below an estimate of the noise level. The photon heights between the high and low limits are considered surface photon heights. To determine the high and low limits, earlier releases compared a smoothed version of the histogram to the median value of the smoothed histogram. Because with the small bin size (1-cm) of the current processing, the median of the smoothed histogram usually reflects the noise tails, and the resulting trimming worked reasonably well. However, it treated the subsurface and above surface tails of the histogram the same.

Because the blue-green laser of ATLAS penetrates water, true subsurface returns have always been a concern, and the higher subsurface density of photons apparent in Figure 1 may be due in part to subsurface scattering in the ocean. However, we see similarly enhanced subsurface densities over, clear deep ocean waters and even over land where penetration and backscatter shouldn't occur. Consequently present thinking expressed in the ATL03 known issues is that the subsurface noise level is due, at least in part, to forward scattering delays in the atmosphere of surface reflected photons.

Whatever their cause, some subsurface photon heights are included in the raw surface height histogram, creating what was an order 1-3 cm bias in average SSH in previous releases. To reduce the sensitivity to subsurface returns, the ASAS code for Release 4 bases surface finding not on a histogram of raw surface height, but on the photon height anomaly about an 11-point moving average of the high confidence photons (confidence level from ATL03 greater than or equal to 3). This moving average does a reasonable job of following large surface waves so that anomalies from it can distinguish subsurface returns versus returns from the troughs of large waves. The Release 4 processing makes a simple estimate of the high and low limits of the anomaly histogram and then uses these to determine separate above surface and subsurface noise levels. The ultimate high limit is then chosen where the smoothed anomaly histogram falls below a factor (e.g., 1.5) times the above surface noise and the low limit is chosen where the smoothed histogram falls below the same factor times the subsurface noise. In testing this approach eliminates more subsurface returns, particularly under wave crests, than were excluded in prior releases with surface finding based on the photon height histogram rather than height anomaly histogram..

Issue 2. Uncertainty in Mean SSH

We have found the wave environment, rather than instrumental factors, is probably the biggest contributor to uncertainty in estimates of the mean SSH. This is illustrated by our analysis of multiple ocean segments, of which the data of Figure 1 is one 7-km ocean segment in the southern part of the central North Pacific. These segments show variability in their mean sea surface heights of approximately ± 0.12 m, much greater than we'd expect from instrumental factors. The standard error, σ_L, in the estimates of the mean are given by

$$\sigma_L = \sigma_h \left(N_{df} \right)^{-1/2}$$

where σ_h is the standard deviation of the population and N_{df} is the number of degrees of freedom. If every one of the ~ 8,000 photon heights were independent, even with a SWH = 2.5 m (σ_h = .625 m), the uncertainty in estimates of the mean would be less than 1 cm. The problem is that owing to the presence of long large waves, successive photon heights are far from independent. The fact that the underlying wave signal is periodic makes the estimate of the effective degrees of freedom problematic. As a worst case if we set N_{df} equal to the number of wave periods in the ocean segment, 15 in the case Figure 1, the uncertainty, σ_L, in the estimate of the mean equals 0.16 m, close to what we see over many similar ocean segments. This problem is not instrumental; it is just made apparent by the ability of ICESat-2 to resolve waves.

To lower this uncertainty, we explored using harmonic analysis of surface height over each ocean segment and use of the zero wave-number amplitude to represent SSH (D. Percival, personal communication, 2019) as a way of removing large periodic variations in height as a cause of uncertainty. This approach did not make a significant difference in ocean segment average sea surface heights. The uncertainty is inherent in measuring SSH over a wave-covered surface. However, the harmonic analysis is included in ATL12 Release 4 to add a measure of wave spectral properties.

Estimates of effective degrees of freedom and uncertainty in Release 4 are based on an autocorrelation analysis of 10-m along-track binned surface heights each ocean segment. These properly account for uncertainties in the ATL12 ocean segment averages of SSH and DOT and will be used in derivation of the ATL19 gridded DOT product.

Issue 3. Erroneous Downlink Bands

In order to conserve bandwidth over the ocean, the Flight Science Receiver Algorithms (FSRA) on board ICESat-2 selects photons in a downlink band currently 50-m in vertical width (See ATL03 Users Guide). This band is centered over where FSRA detects the highest concentrations of photons. Signal confidence equal to 2, 3, 4 correspond to low, medium, and high confidence that the photon is a surface return. Signal confidence equal to 1 is applied to the remaining no confidence photons filling a band ±30-m around the high confidence photons. As long as the background photon count is low at night or in clear conditions this band will be centered on the ocean surface near the geoid. But in daylight with scattered clouds, the downlink band can shift to unrealistic heights or depths for 200-pulse major frames. To reduce this problem, for Release 4 and beyond, ATL03 only keeps downlinked photons within 30 m of DEM, or geoid in the case of the ocean. In any event, to avoid erroneous downlink bands, the ATL12 Release 4 ASAS code selects a band that includes photons with a signal confidence greater than or equal to 1 and falling within ±15-m of the EGM2008 geoid.

Issue 4. Sea Surface Heights Among Beams

Our cal/val comparisons with CryoSat-2 (Figs. 4 and 5) had been performed for the center strong beam only. In developing the ATL19 gridded product processing we experiment with gridding DOT separately for each beam. For an ATL12 derived from an experimental ATLO3 made with the current orbit and pointing determinations as used in ATL03 Release 4 and beyond, we find the biases between all but one of the beams are less than 1 cm.

Issue 5. Bathymetry Test and Surface Type

As mentioned in the notes, releases after Release 3 include a bathymetric test based on GEBCO ocean depth greater than 10-m to insure the ATL12 processing covers only ocean waters. It also includes ocean segment average depth as an output. The user can gain an appreciation of how much non-open ocean is included in an ocean segment by looking at the *gtxx/ssh_segments/stats/surf_type_prcnt* output variable that gives the percentage of the ocean segment covered by each surface type covered in an ocean segment. (Be advised that the surface type from 1 to 5 denote land, ocean, sea ice, land ice, and inland water as listed in ATL03).

Issue 6. SSB Calculation

We estimate the Sea State Bias (SSB) due to variations in sampling over surface waves. The electromagnetic (EM) sea state bias occurs for example if more photons tend to be returned from wave troughs than from wave crests. This SSB is equivalent to the covariance of photon return rate and sea surface height divided by the average photon return rate. We estimate this with the return rates and heights averaged in 10-m along track bins. The SSB estimates have been smaller than we have expected ~-1.2 % of Significant Wave Height (SWH). Note that the SSB parameter is an estimate of sea state bias and should be subtracted from the heights output by ATL12 Release 4 to correct the heights for sea state bias. Also note, typical radar altimeters show an SSB of about – 4% and we have found ICESat to have no SSB below SWH= 2 m, but -18% of SWH above 2 m [*Morison et al.*, 2018]. ICESat-2 appears to be less sensitive to SSB. Also note, our ICESat-2 SSB is an *a priori* prediction based on EM bias. It doesn't include SSB due to retracker design or assumptions about waveform or surface height distribution. ICESat-2 processing doesn't involve retracking and such assumptions, but testing how well the *a priori* EM bias represents total ICESat-2 SSB is worthy of further research.

Issue 7. Quasi-specular returns and possible first-photon bias

Related to the SSB calculation issue, ATL07 results near the ice edge sometimes show reduced SSH near the ice edge. It has been hypothesized that this is due to quasi-specular returns from the troughs of waves. We see some evidence of these depressions in the ATL12 data along the East Greenland ice edge, but have not as yet tested this hypothesis with our SSB calculation.

Occasionally we see regions of photon return rates ten times higher than normal in the open ocean. These regions of quasi-specular returns are usually areas without large wind waves, and we think they are also areas where small ripples effectively broaden the angular dependence of reflectance just enough to give strong returns within a few degrees of nadir incidence. This may result in positive height bias over surfaces producing quasi-specular returns.

Not anticipating such high reflectance from the ocean, we have not implemented a correction, *fpb_corr*, for photon detector saturation induced first photon bias in ATL12. As a place-holder, *fpb_corr* is currently being set to INVALID_R4B in ATL04. Release 4 does average the saturation flags as by *full_sat_fract_seg* and *near_sat_fract_seg.*.

Associated with saturation, photon after-pulses produce false subsurface return peaks. In the Release 4 ATL12 processing, photons in these after-pulses are edited out by considering only photons with the index of photon height quality from ATL03 (*quality_ph*) equal to 0. In future releases (Release 5) we will delete all photons coming from laser pulses that include any photons with a quality index indicative of saturation, or we will consider applying a TBD first-photon-

bias correction if there are ocean segments for which the fraction of saturated photons is high as indicated by *full_sat_fract_seg* and *near_sat_fract_seg.*

Issue 8. Lower transmitted energy in Beam 3 (Strong Beam)

According to the ATL07/10 results, the transmit energy of Beam 3 (Strong beam 2R or 2L, depending on orientation of the ICESat-2 observatory) is approximately 80% that of Beam 1 and Beam 5. Thus, the segment lengths and photon return rate for Beam 3 may be different from the other two strong beams.

Issue 9. Ice versus Sea Surface Height in Sea Ice Covered Regions

Sea ice regions fall under the Sea Ice Surface mask where sea ice surface height (ATL07), and freeboard and sea surface height anomaly (ATL10) are determined. The sea ice surface mask is defined as that part of the ocean where sea ice concentrations (from passive microwave remote sensing) are greater than 15%. However, sea ice regions also fall under the ocean mask. Consequently, the user will find ATL12 sea surface heights in ice-covered regions, and these will be biased above the true sea surface height by approximately the freeboard of the ice from ATL10. As with Issue 5, the user can gain an appreciation of how much sea ice is included in an ATL12 ocean segment by looking at the *gtxx/ssh_segments/stats/surf_type_prcnt* output variable that gives the percentage of the ocean segment covered by each surface type in an ocean segment. In the ATL19 gridded ocean product in ice covered regions, we will ultimately combine the ATL 10 and ATL12 surface heights to produce a merged, all-ocean monthly gridded sea surface height and an estimate of ice concentration as well.

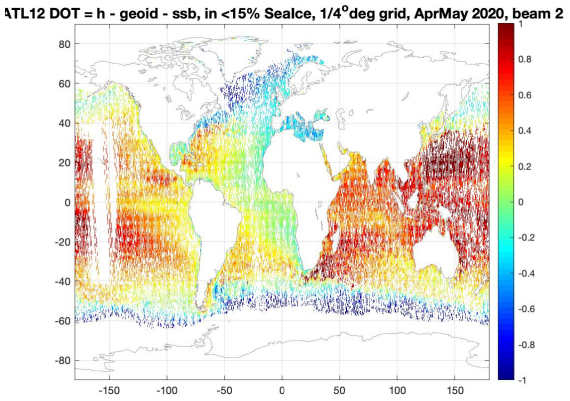

Figure 6. ATL12_2020**0401**021904_00850701_003_01.h5 to ATL12_2020**0513**123852_07330701_003_01.h5 DOT averaged in ¼° bins for sea ice concentration <15%.

Issue 10. Spikes in ATL12 DOT and SSH Values

Dynamic ocean topography (DOT), in addition to being the determinant of surface geostrophic circulation, provides an excellent check on the final ATL12 sea surface height product. DOT is equal to sea surface height corrected for sea state bias minus the geoid (*gtxx/SSH_segment/heights/h - gtxx/SSH_segment/heights/bin_ssbias - gtxx/SSH_segment/stats/geoid_seg*)*. Reasonable values are within a meter or two of zero, and in the current release this is mainly true world-wide (Fig.6) but there are unrealistic spikes in DOT (Fig. 7). These seem to come in two varieties.

a) We find numerous large DOT spikes (order several meters) near the ice edges (Fig. 7 upper in blue). These are likely rough ice signatures. They are especially bad in the Antarctic seasonal sea ice zone and we find the larger spikes are due to returns off ice shelves and icebergs, which are included in the ocean mask.

b) At mid and tropical latitudes (Figure 7 upper in red), there are spikes that we have learned are associated with maneuvering the ICESats-2 spacecraft in Drag Make Up (DMU) operations. We see about 5-6 DMUs per month lasting about an hour each and when they occur they may affect 10-15% of the ocean segments in the ATL12 file so afflicted. In Release 4 we use the *pod/ppd_flag* to edit the data. A list of DMUs for the entirety of the mission is provided for end users to see at NSIDC, and the times of these can also be used to delete particular ocean segments.

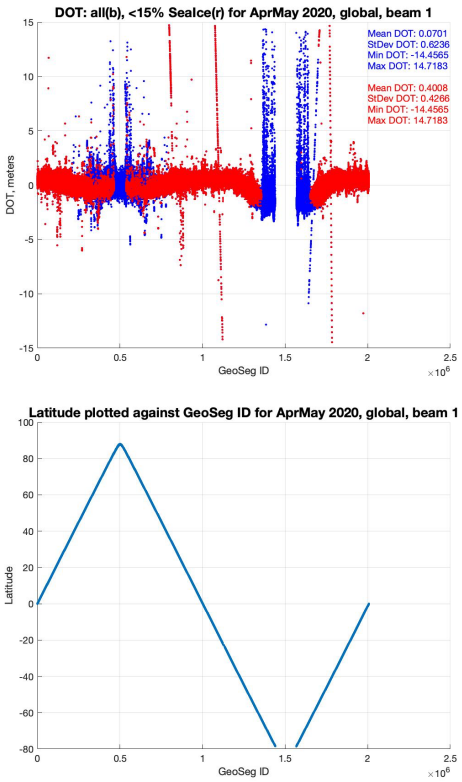

Figure 7. DOT versus ocean segment ID (upper) and ocean segment latitude versus ocean segment ID (lower).

c) Related to item b) ICESat-2 performs conical "Ocean Scans" to check the pointing calibration. These are commonly over the western Pacific. During the scans, the incidence angle is increased to 5° and we find the heights develop substantial inter-beam biases and should not be used for ocean height measurement. Consequently, users are advised to ignore any ocean segment heights for which the incidence angle indicated by the elevation angle, *ref_elev_seg*, is greater than 2°, i.e., when abs(90° - *ref_elev_seg* * 180°/□) > 2°

d) In separate work, looking at ATL12 DOT around Greenland, we also found unrealistic spikes in sea surface height that may or may not be due to ice or POP/PPD issues. To avoid these getting into the ocean gridded product, ATL19, we will pre-filter ATL12 data with a 2-pass, 3-sigma filter on DOT. This is may be a good overarching approach for other ATL12 users as well.

* Note: The description for ocean segment sea state bias, *gtxx/SSH_segment/heights/bin_ssbias*, in Release 3 was incorrect reading:
" Mean of linear fit removed from surface photon height (4.3.1)"
In Release 4 it should read:
"Ocean segment EM sea state bias computed from correlation of 10-binned surface photon rate and surface height. It is on the order of cm and should be subtracted from *gtxx/SSH_segment/heights/h* to correct for sea state bias."

Issue 11. Photon Noise Rate

ASAS implementation of photon noise rate does not agree with the intent of the Ocean ATBD. ASAS computation of *n_photonns*, now termed *photon_noise_rate*, includes all downlinked photons with signal confidence < 1, or a too shallow depth, or *quality_ph* that is not zero. The ATL12 ATBD only considers photons in the band within ±15-m of the EGM2008 mean tide geoid.

Issue 12. Surface Type Percent Scaling

The ocean segment average surface type percentage for ocean, *surf_type_prcnt*(2), should equal 100% because an ocean depth criteria, depth > 10 m, is used to decide where to compute ocean segment averages. Because of overlap regions between the various surface masks, there can also be significant percentages of other surface types less than or equal to 100%. However, we have found that the surf_type_prcnt values have a scaling error on rel005, ATL12 product such that the ocean surface type percentage is always less than 100%. Other surface type percentages are similarly reduced. To obtain corrected surf_type_prcnt values, first compute a scale factor (sf) by:

sf = 1 / (Oc_prcnt / 100),

where Oc_prcnt is the ocean surface type percentage (second column of *surf_type_prcnt*, *surf_type_prcnt*(2). This scale factor, sf, is used as a multiplier for all *surf_type_prcnt* values for that specific ocean segment.

This scaling will always yield a corrected value for ocean surf_type_prcnt of 100%. Non-ocean surface types will commonly have values of zero or 100%, with occasional values falling in between, for those segments located in a surface type mask transition zone.

Reference:

Morison J., R. Kwok, S. Dickinson, D. Morison, C. Peralta-Ferriz, and R. Andersen (2018), Sea State Bias of ICESat in the Subarctic Seas, *IEEE Geoscience and Remote Sensing Letters*, 15 (8), 1144 - 1148, DOI: 10.1109/LGRS.2018.2834362